Patrick Hubert Wagner	Wagner	mail@patrick-wagner.net
First	*Last*	*E-mail*

ASME Paper Title: Theoretical and Experimental Investigation of a Small-Scale, High-Speed, and Oil-Free Radial Anode Off-Gas Recirculation Fan for Solid Oxide Fuel Cell Systems

Authors: Patrick Hubert Wagner, Jan Van herle, Jürg Schiffmann

ASME Journal Title: ASME Turbo Expo 2019: Turbomachinery Technical Conference and Exposition
June 17–21, 2019, Phoenix, Arizona, USA

Paper No°: GT2019-91361, V008T26A019; 12 pages **Date of Publication (VOR* Online):** November 5, 2019

ASME Digital Collection URL:
https://asmedigitalcollection.asme.org/GT/proceedings-abstract/GT2019/58714/V008T26A019/1067197

DOI: https://doi.org/10.1115/GT2019-91361

*VOR (version of record)

A modified version was also published in the Journal of Gas Turbines and Power
Infoscience: https://infoscience.epfl.ch/record/271135?ln=en
DOI: http://dx.doi.org/10.1115/1.4045104

PRE-PRINT

DRAFT: THEORETICAL AND EXPERIMENTAL INVESTIGATION OF A SMALL-SCALE, HIGH-SPEED, AND OIL-FREE RADIAL ANODE OFF-GAS RECIRCULATION FAN FOR SOLID OXIDE FUEL CELL SYSTEMS

Patrick H. Wagner
Laboratory for Applied Mechanical Design (LAMD)
Institute of Mechanical Engineering (IGM)
École Polytechnique Fédérale de Lausanne (EPFL)
Neuchâtel, Neuchâtel, 2000
Switzerland
Email: patrick.wagner@epfl.ch

Jan Van herle
Group of Energy Materials
IGM
EPFL
Sion, Valais, 1951
Switzerland
Email: jan.vanherle@epfl.ch

Jürg Schiffmann*
LAMD
IGM
EPFL
Neuchâtel, Neuchâtel, 2000
Switzerland
Email: jurg.schiffmann@epfl.ch

ABSTRACT

The Laboratory for Applied Mechanical Design (LAMD) designed, manufactured, and experimentally tested a novel recirculation fan for a $10\,\mathrm{kW_e}$ *Solid Oxide Fuel Cell (SOFC). The fan uses oil-free bearings, more specifically herringbone-grooved journal and spiral-grooved thrust gas bearings. The radial inducer-less fan with a tip diameter of* $19.2\,\mathrm{mm}$ *features backward-curved prismatic blades with constant height. Prior to coupling the recirculation fan with the SOFC, the fan was experimentally characterized with air at* $200\,^{\circ}\mathrm{C}$*. At the nominal point of* $168\,\mathrm{krpm}$*, the measured inlet mass flow rate is* $4.9\,\mathrm{kg\,h^{-1}}$*, the total to total pressure increase* $55\,\mathrm{mbar}$*, the isentropic total to total efficiency* $55\,\%$*, and the power* $18.3\,\mathrm{W}$*. This paper compares the experimental data towards a computational fluid dynamic simulation of the full fan impeller and volute suggesting an excellent agreement at the nominal point which validates the numerical approach. However, the heat flows crossing the fan fluid domain, have an increased effect at off-design conditions, thus the experimental results need careful consideration. The fan backface leakage has negligible impact on the measurements.*

*Address all correspondence to this author.

NOMENCLATURE

b (Channel) width m
c Clearance in m
d, D Diameter in m
h Specific enthalpy in $\mathrm{J\,kg^{-1}\,K^{-1}}$
l Length in m
M Torque in $\mathrm{N\,m}$
$\dot{m}$ Mass flow rate in $\mathrm{kg\,s^{-1}}$
P Power in W
p Pressure in Pa
$\dot{Q}$ Heat rate in W
T Temperature in K
t (Blade) thickness in m
β Blade angle based on the circumference in $^{\circ}$
γ Molar fraction
η Efficiency
ω Angular speed in $\mathrm{rad\,s^{-1}}$

Subscript

1 Machine inlet / inlet side test section
3 Fan blade leading edge
4 Fan blade trailing edge
8 Machine outlet / outlet side test section
a axial
amb ambient

cond conduction
is isentropic
l leakage
n nominal
s shroud
st static
t total

Abbreviation

AOR Anode Off-gas Recirculation
DLC Diamond-Like Carbon
TE Trailing Edge
SOFC Solid Oxide Fuel Cell

INTRODUCTION

Intermediate-temperature Solid Oxide Fuel Cells (SOFCs) have proven to be efficient and reliable: The commercial product BlueGEN with a net output power of 1.5 kW_e reaches net efficiencies based on the lower heating value of methane of 60 % and utilization ratios that take into account the cogeneration of electricity and low-temperature heat of 85 % [1]. An SOFC prototype equipped with a similar technology as used by the BlueGEN has achieved recently more than 90 000 h of continuous operation at the German research center "Forschungszentrum Jülich" [2].
Wagner et al. [3] simulated and optimized a 10 kW_e SOFC system with anode off-gas recirculation (AOR). Their conclusion is that an electrical net efficiency of up to 64.9 % and a utilization ratio of up to 97.2 % are theoretically possible. Peters et al. [4] experimentally demonstrated the technical feasibility of a 2.5 kW_e SOFC stack with AOR reaching an electrical net efficiency of 58.5 %. They claim that if a new stack had been used instead of an aged one the efficiency would have been at least 5 points higher. The results therefore suggest that net efficiencies in the order of 65 % are within reach for an SOFC systems coupled with anode off-gas recirculation devices. Although the mentioned SOFC systems are at domestic scale with a power output of a few kW_e, their efficiencies are comparable with state-of-the art combined-cycle power plants which deliver electrical power in the order of several hundreds of MW_e. As of September 2018, the world record for combined-cycle power plants is 63.1 % [5]. An additional advantage of the SOFC is the locally cogenerated heat, which domestic heating or cooling can use, hence increasing the system utilization ratio. Cogeneration of electricity and heat is very promising for decentralized energy integration in residential and commercial markets.

THE ANODE OFF-GAS RECIRCULATION FAN

AOR needs a recirculation device to overcome the pressure losses within the SOFC system. Besides fuel-driven and steam-driven ejectors, fans are very common. Wagner et al. [6] compare four different devices that the literature provides including fans with ball bearings that are coupled to an electric motor with a magnetic coupling, as well as directly coupled fans with ball bearings, dynamic oil film bearings, or dynamic gas film bearings. The latter option has the advantage of grease and oil-free operation, resistance to high temperatures, and a long life time which makes this concept particularly interesting for this application. Previous and current projects [7, 8] use foil journal and axial thrust bearings as dynamic gas film bearings.

TABLE 1. GEOMETRICAL PARAMETERS OF THE RADIAL ANODE OFF-GAS RECIRCULATION FAN, ADAPTED FROM [6].

Impeller (4+4 prismatic blades)		
Blade leading edge (3) at hub and shroud (s)		
d_{3hub}	7.32 mm	d_{3s} 10.02 mm
$\beta_{3,blade}$	36° (hub) to 30° (shroud)	(blunt leading edge)
Blade trailing edge (4)		
d_4	19.20 mm	t_{blade} 0.25 mm
b_4	1.82 mm+0.15 mm	(shimmed)
$\beta_{4,blade}$	17°	(cut-off trailing edge)
Blade tip clearance (c)		
c_{nom}	0.05 mm	(nominal)
c_{shim}	0.05 mm+0.1 mm	(shimmed)
Fan backface clearance (c)		
c_a	0-0.011 mm	(axial thrust bearing)

Wagner et al. [6] present the design of a novel radial recirculation fan whose design is a trade-off between efficiency and low manufacturing cost. Table 1 lists some geometrical parameters such as diameters (d), blade angles (β) based on the circumferential component, channel width (b), blade thickness (t), and clearances (c). The fan design matches the mass flow rate and pressure rise requirements of a 10 kW_e SOFC and its design parameters at the machine inlet (1) are as follow: total pressure ($p_{t,1}$=1.05 bar), total temperature ($T_{t,1}$ =200 °C), mass flow rate ($\dot{m}_1$=4.78 kg h^{-1}), as well as the molar ratios of water vapor, hydrogen, carbon monoxide, and carbon dioxide (γ_i =61.4 %,

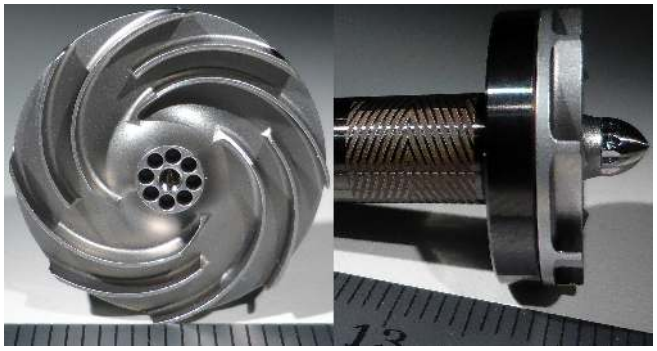

FIGURE 1. FRONT AND SIDE VIEW OF THE ANODE OFF-GAS RECIRCULATION FAN, ADAPTED FROM [6] (1 TICK = 1 MM).

7.4 %, 2.6 %, and 28.6 %). The design total to total pressure increase over the fan is 70 mbar at a design rotational speed of 175 krpm. Figure 1 shows the manufactured and tested fan. A Diamond-Like Carbon (DLC) coating protects the 8 mm shaft to reduce the friction and wear during the fan startup and shutdown. The rotor features two herringbone-grooved journal bearings (only one visible in Figure 1 on the right) and one single-sided spiral groove thrust bearing that is located on the fan backside (not visible in Figure 1). The thrust bearing operates in the pump-in mode, i.e. it draws the gaseous lubricant from the blade trailing edge (TE) into the fan housing.

MEASUREMENT SETUP

Prior to the actual coupling with the SOFC, the authors performed several experiments at their facilities: balancing of the machine up to design speed (175 krpm), measurement of axial shaft displacement (without fan volute), fan operation with air at ambient temperature, and finally with hot air at 200 °C. It should be noted, that a partial admission, low-reaction, radial-inflow, 15 mm turbine propels the shaft and thus the fan.

Figure 2 shows the setup of the test rig for the hot air tests at 200 °C. The prototype with all measurement sensors is inside a ceramic oven (volume of 60 l) that is maintained at a constant temperature of 200 °C simulating the actual environment of the AOR fan in the SOFC hot box. The fan test temperature of 200 °C is a trade-off between the maximum temperatures for the shaft DLC coating (∼250 °C), maximum temperature of high-temperature plastics (∼260 °C) such as PTFE and FFPM, as well as considering the whole SOFC system design. Results by Wagner et al. [3] suggest that a low-temperature AOR at 200 °C leads to a higher SOFC electrical net efficiency compared to a hot recirculator operating at ∼750 °C, but complexifies the system by adding an additional heat exchanger that cools the anode off-gas from its exhaust temperature (∼750 °C) to the AOR fan inlet temperature. In addition, the lowest AOR temperature should be above the dew point temperature of the water vapor in the anode off-gas, since condensation leads to the formation of acids.

Since the volume of the oven is small and the fan ingests hot air air directly from the oven volume, an air preheating system supplies the oven with excess hot air at 200 °C. The hot air distributor injects the preheated air into the oven parallel to the oven bottom (see lowest red arrow in Figure 2) to lower the vertical temperature gradient within the oven.

The fan test setup inside the oven refers to the standard test methods with outlet side test ducts - category B test installation with inlet duct (category D) of the ISO 5801 [9]. With respect to this norm, the test rig in Figure 2 and Figure 3 features several differences:

- Fan inlet volume flow rate measurement with a bellmouth
- Fan inlet temperature measurement (3x)
- Fan outlet temperature measurement (2x)
- No shaft torque measurement

The shaft torque measurement of such a small-device is complicated due to various reasons: (1) the shaft diameter is with 8 mm very small, (2) the dynamic gas film bearings with a radial clearance in the order of several µm have a low load capacity and a low tolerance to displacement or misalignment, (3) the torque is between 0 to 0.001 N m and therefore very low, (4) the temperatures are with 200 °C elevated, and (5) the available place for any measurement device is restricted to a few millimeters. To the authors knowledge, no torque measurement devices which complies with the above mentioned specifications is available so far. Thus, the fan power was measured thermodynamically with the fan inlet and outlet temperatures, as well with the measured inlet mass flow rate.

Class 1 k-type Thermocouples with a 1.5 mm diameter measure the temperatures. Three equally-distributed thermocouples are placed at $3d_1$ (d_1 =12 mm) upstream of the fan inlet nozzle and measure the average fan inlet temperature. Two thermocouples are placed at the fan outlet after the static pressure measurement

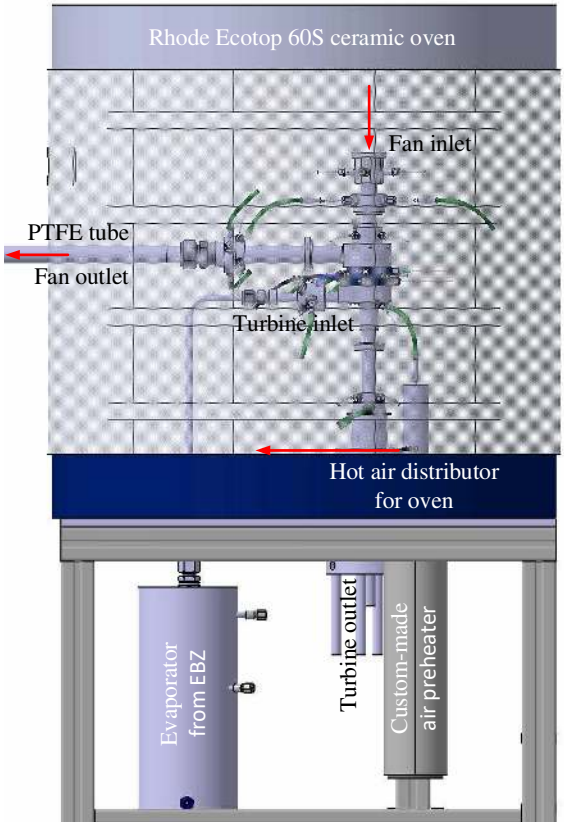

FIGURE 2. OVERVIEW OF THE THE FAN TEST RIG FOR HOT AIR AT 200 °C (WITHOUT GLASS FIBER ISOLATION).

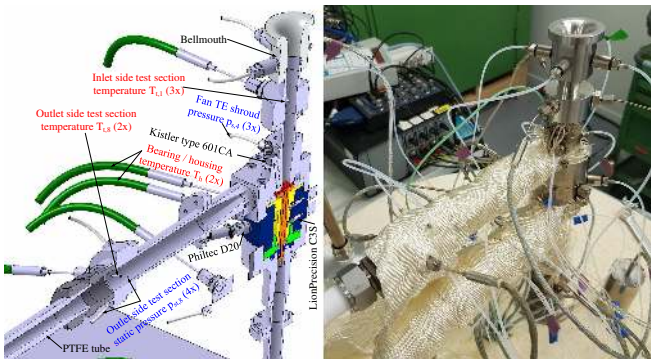

FIGURE 3. CAD OF THE FAN TEST RIG WITH MEASUREMENT POSITIONS (LEFT) AND REAL IMPLEMENTATION (RIGHT), PARTLY COVERED WITH GLASS FIBER ISOLATION.

for obtaining the average fan outlet temperature (see Figure 3). In order to limit the heat conduction effects between the thermocouples and the oven environment the latter are imerged five-times their diameter into the exhaust flow. The heat conduction of the metallic outlet side test section itself to the environment is limited by decoupling it with a PTFE tube (see Figures 2 and 3).

Since thermodynamic measurements determine the fan power, an adiabatic system is essential. Thus, high-temperature glass fiber isolation wrapped around the fan body and pipes inside and outside the oven limit the heat loss. Figure 3 shows these glass fiber tapes for the outlet side test section.

The test rig features four additional thermocouples: one at the top of the oven, one inside the volume flow rate measurement device in the outlet side test section (fluid outlet density calculation), and two inside the fan housing close to the journal bearings (see Figure 3).

An *MKS* 226A (0.133 bar) differential capacitance manometer measures the differential pressure between the fan outlet (four pneumatically-averaged static pressure measurements) and the oven. A *Scanivalve* DSA 3218 (17.24 bar) measures the gauge pressures inside the oven, before the volume flow rate measurement device at the outlet (fluid outlet density calculation), inside the fan housing, and at the fan TE (3x). The fan volute features three equally-distributed static pressure measurements with a diameter of 0.4 mm located at a diameter of 18.55 mm (the fan TE is 19.2 mm). The first is located at 0° coinciding with the end of the volute logarithmic spiral and thus the volute outlet section (see Figure 10). A *Lufft* Opus 20 room climate tracker measures the ambient pressure.

A low-ratio long radius bellmouth according to ISO 5167-3 [10] limits the pressure loss at the fan inlet. An *MKS* 223B (0.01 bar) measures the differential pressure between the bellmouth (four pneumatically-averaged static pressure measurements) and the oven environment, thus allowing to calculate the fan inlet volume flow rate ($\dot{V}_1$). Since the inlet Reynolds number based on the outer bellmouth diameter (Re_D) is smaller than the limit value in the ISO 5167 norm, the implemented bellmouth has been calibrated with the volume flow rate measurement device at the fan outlet.

An orifice plate with wall taps in accordance to ISO 5167-2 [10] measures the fan outlet volume flow rate. For low Reynolds applications, quarter circle nozzles are preferred to orifices with sharp edges such as stated within ISO 5167-2. The discharge coefficient of quarter circle nozzles is nearly constant down to Reynolds numbers based on the outer diameter (Re_D) of 500. The VDI/VDE 2041 [11] is an addition to the ISO 5167 and states norms for such quarter circle nozzles. Like for the bellmouth at the fan inlet, the quarter circle nozzle at the fan outlet with an outer diameter (D_8) of 12 mm is well below the minimum value in VDI/VDE 2041 (50 mm). Hence, the supplier *Tetratec* calibrated it. An *MKS* 226A (0.133 bar) measures the quarter circle nozzle differential pressure.

In order to deswirl the fan exhaust flow a cross-shaped flow straightener with an length to diameter ratio ($l/D_8 = 24/12$) of 2 is placed at $45D_8$ after the fan volute outlet diffuser, a Zanker flow conditioner plate at $63D_8$, and the quarter circle nozzle at $93D_8$ (devices not visible in Figure 2).

Figure 3 shows the three devices for the shaft rotational speed measurement:

1. Lion Precision C3S capacitive probe (not usable at 200 °C)
2. A high-temperature *Philtec* D20 optical probe
3. A high-temperature *Kistler* Type 601CA piezoelectric pressure sensor measuring the blade passing frequency at the blade TE (diameter of 18.55 mm)

Options 1 to 3 show coherent measurements at ambient temperatures. Figure 4 shows an example: The C3S measures the rotor orbit in one direction ($2608 \cdot 0.06 = 168.48$ krpm), the Philtec D20 two grooves on the shaft ($\frac{5615}{2} \cdot 0.06 = 168.45$ krpm), and the pressure sensor the blade passing frequency of the eight blades ($\frac{22458}{8} \cdot 0.06 = 168.435$ krpm). The option 2 and 3 are imple-

TABLE 2. MEASUREMENT UNCERTAINTIES.

Temperature		
Thermocouple	±0.5 °C, Calibration (Cal.)	
Pressure		
Scanivalve	±0.018 % of the full scale (FS)	
MKS	±0.3 % on the read (OR)	
Ambient	±0.5 mbar	
Volume flow rate		
Bellmouth	±0.96 % OR / ±0.3 % OR	Cal. / *MKS*
Quarter circle nozzle	±0.91 % OR / ±0.3 % OR	Cal. / *MKS*
Rotational speed		
Philtec D20	±0.5 krpm (@ 50 kHz sampling)	
Displacement		
LionPrecision C3S	±0.25 % FS	

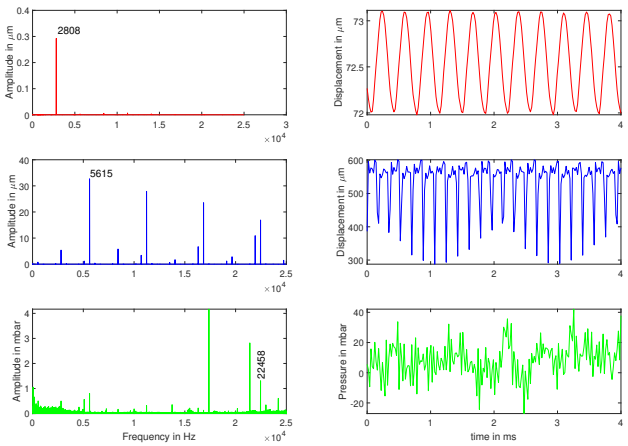

FIGURE 4. ROTATIONAL SPEED AT 168.5 KRPM MEASURED WITH THE LIONPRECISION C3S PROBE (RED), THE PHILTEC D20 PROBE (BLUE), AND THE KISTLER 601CA (GREEN) IN THE FREQUENCY DOMAIN (LEFT) AND TIME DOMAIN (RIGHT).

mented for the measurement at high temperatures of 200 °C. Table 2 shows the measurement uncertainties of the temperature, pressure, volume flow rate, rotational speed, and displacement measurements. It should be noted that the measurement uncertainty of the *Scanivalve* is relatively high (±3.1 mbar). However, both the Scanivalve and the MKS measure the fan pressure rise and both show coherent output within ±0.8 mbar. The authors assume therefore the *Scanivalve* measurement accuracy as sufficient.

FAN EFFICIENCY AND POWER MEASUREMENTS

As pointed out in the previous section, a shaft torque measurement is not possible due to several restrictions. Thus the fan power and efficiencies are evaluated thermodynamically via the fan inlet and outlet temperatures, as well as the inlet mass flow rate. Figure 5 shows the fan impeller domain with its boundaries marked with a green-dashed line. Several enthalpy, power, and heat fluxes cross the control volume boundaries. At the fan inlet (1) and outlet (8) the measurement of mass flow rate, temperature, and pressure allow for the determination of the enthalpy.

While considering all energy fluxes shown in Figure 5 the stationary energy balance is given as follows.

$$P_{fan} + \dot{m}_1 h_{t,1} - \dot{m}_8 h_{t,8} + \dot{m}_l h_{t,l} + \dot{Q}_{cond} - \cancel{\dot{Q}_{amb}} - \cancel{M_{z,s}\omega} = 0 \quad (1)$$

The nominal fan tip clearance is set to 50 µm. However for risk mitigation, the first tests use a 100 µm shim (see Figure 5) that increases the fan blade tip clearance to 150 µm, yielding a relative running blade tip clearance of 0.071 ($\frac{c_4}{b_4} = \frac{0.139}{1.959}$) at 168 krpm. A high relative tip clearance decreases the fan efficiency due to increased tip leakage and reduces the fan pressure increase. An increased tip clearance also reduces the shroud torque ($M_{z,s}$). The efficiency calculation assumes an adiabatic fan shroud, i.e. the viscous losses due to the shroud torque increase only the temperature of the fan fluid. Hence $M_{z,s}\omega$ in eq. (1) is approximately zero. The values obtained with numerical simulations suggest that the shroud torque power ($M_{z,s}\omega$) may reach 5 % of the fan power (non-throttled case at 168 krpm).

Both the leakage mass flow rate from the housing to the fan fluid domain and heat dissipation from the thrust bearing may affect the power and efficiency measurements significantly:

• The leakage mass flow rate from the pressurized housing (due to the turbine) towards the fan TE corresponds to the difference between the fan outlet and inlet mass flow rate ($\dot{m}_l = \dot{m}_8 - \dot{m}_1$). The leakage flows from the housing through the in-ward pumping axial thrust bearing, and enters the fan impeller fluid domain at the TE (see white arrows in Figure 5). Figure 11 shows the static housing pressure that is equal to to the total pressure (fluid velocity near zero), as well as the fan TE shroud pressure at 0°, 120°, and 240°. Since the fan power is deduced from the mass flow rate and temperature measurements, the leakage flow temperature has a direct impact on the measured fan power. If the leakage flow temperature is higher than the fan inlet temperature, the actual measurement overestimates the fan power and thus underestimates the fan efficiency (and vice versa) for the case the fan inlet mass flow rate evaluates the fan power

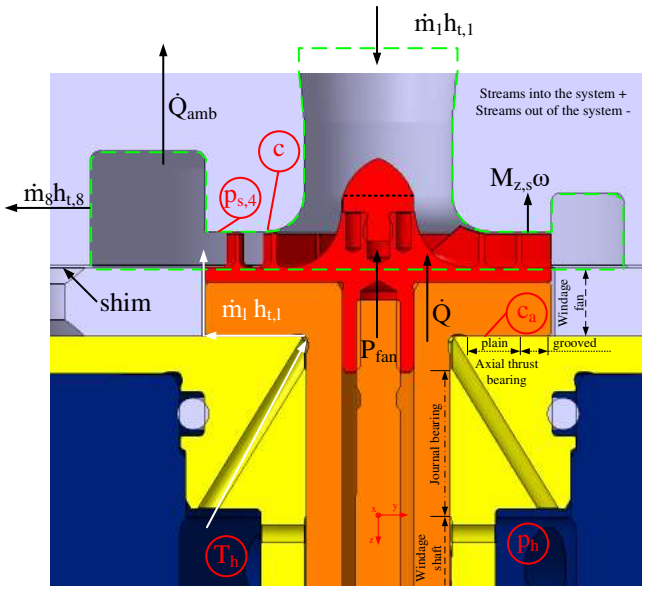

FIGURE 5. OVERVIEW OF ENTHALPY, POWER, AND HEAT INPUT, RESPECTIVELY OUTPUT TO THE FAN MEASUREMENT SYSTEM.

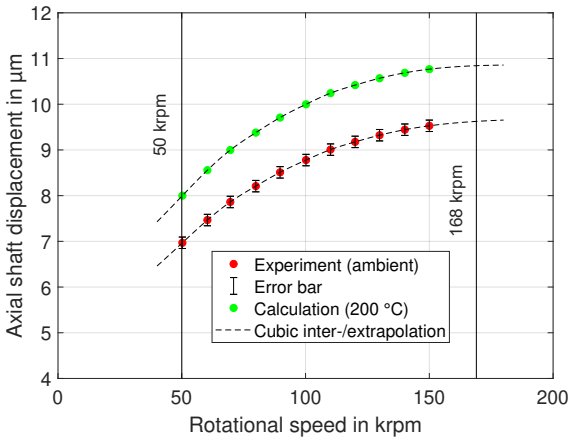

FIGURE 6. MEASURED AND CALCULATED AXIAL SHAFT DISPLACEMENT WITHOUT MOUNTED FAN VOLUTE.

($P_{fan} = \dot{m}_1 (h_{t,8} - h_{t,1})$).

• The heat input to the fan impeller ($\dot{Q}$) has mainly two sources: (1) the heat conduction within the shaft because of a temperature gradient between the fan and the housing, respectively the turbine, as well as (2) the more dominant heat dissipation due to the losses of the journal bearings, the thrust bearings, and the shaft windage (see Figures 5 and 8). This heat dissipation is directly linked to the viscous losses and thus losses which can be experimentally determined with a shaft run-out test. The heat conduction to the environment ($\dot{Q}_{amb}$) in eq. (1) is approximately zero because of the glass fiber isolation.

As a consequence of this, this paper evaluates three different isentropic total to total fan efficiencies.

$$\eta_{is,1} = \frac{\cancel{\dot{m}_1} (h_{t,8,is} - h_{t,1})}{\cancel{\dot{m}_1} (h_{t,8} - h_{t,1})} = \frac{P_{is}}{P_1} \quad (2)$$

$$\eta_{is,2} = \frac{\dot{m}_1 (h_{t,8,is} - h_{t,1})}{\dot{m}_8 h_{t,8} - \dot{m}_1 h_{t,1} - \dot{m}_l h_{t,l}} = \frac{P_{is}}{P_2} \quad (3)$$

$$\eta_{is,3} = \frac{\dot{m}_1 (h_{t,8,is} - h_{t,1})}{\dot{m}_1 (h_{t,8} - h_{t,1}) - \dot{Q}_{cond}} = \frac{P_{is}}{P_3} \quad (4)$$

A fluid database evaluates the thermodynamic properties for dry air that is assumed as mixture of nitrogen, oxygen, and argon (γ_i =0.78126, 0.2094, 0.00934).

EVALUATION OF THE LEAKAGE FROM THE TURBINE TO THE FAN

Figure 6 shows the shaft axial displacement (c_a) as a function of the rotor rotational speed that is measured with a *Lion-Precision* C3S capacitive probe at ambient conditions (red dots). The probe is mounted vertically above the fan spinner, which for these measurements is flat (black thick dotted line in Figure 5). At elevated temperatures, the viscosity of air increases, hence the load capacity and stiffness of the bearing increase. Figure 6 shows green dots that correspond to the calculated axial clearance at 200 °C, assuming the same axial force for both the ambient and the hot case. The difference between the two cases is around 1 μm. Since space is limited, the axial displacement was only measured without the fan volute.

Figure 7 shows the measured leakage mass flow rate (red line) for the case of a non-throttled fan. The measured leakage mass flow rate from the turbine to the fan is in the orders of several 0.1 kg h^{-1}. The measurement is compared towards an analytical calculation based on a Laval nozzle that takes into account the axial thrust bearing clearance (see green line in Figure 6), the total pressure and temperature in the housing (p_h and T_h), and the average fan TE shroud pressure. The blue line in Figure 7 shows this maximum possible leakage mass flow rate with a theoretical discharge coefficient of 1 ($CD = 1$). This maximum leakage mass flow rate for the non-throttled fan is therefore below 0.2 kg h^{-1} and thus lower than 4 % of the fan inlet mass flow rate for all measured points between 50 krpm to 168 krpm. These results clearly suggest a significant discrepancy between the measurements and the theoretically maximum leakage flow rates. The authors hypothesize that this discrepancy is a consequence of residual swirl within the outlet side test section. As a consequence the efficiency $\eta_{is,2}$ from eq. (3) is evaluated using the calculated maximum possible leakage flow rate (blue line in Figure 7) instead of the measurements. The fan outlet mass flow rate is accordingly calculated with this maximum analytical value for the leakage mass flow rate and the fan inlet mass flow rate ($\dot{m}_8 = \dot{m}_1 + \dot{m}_l$).

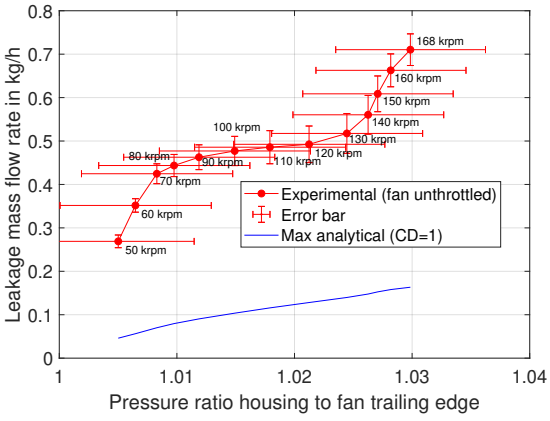

FIGURE 7. COMPARISON OF EXPERIMENTAL AND ANALYTICAL (CD=1) LEAKAGE MASS FLOW RATE FROM TURBINE TO FAN FOR THE NON-THROTTLED FAN OPERATION.

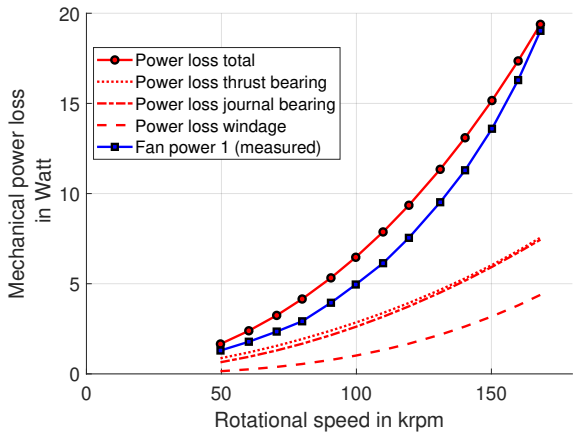

FIGURE 8. CALCULATED LOSSES AND MEASURED FAN POWER AT 200 °C FOR THE MEDIUM THROTTLED CASE.

EVALUATION OF THE HEAT DISSIPATION BY SHAFT LOSSES

Above the lift-off speed, aerodynamic bearings operate without contact to the stator part. Nevertheless, the bearings yield losses due to the viscosity of the gas lubricant within the fluid film. Demierre et al. [12] compared an analytical windage loss model to rotor run-out measurements of a micorcompressor-turbine unit and suggest good agreement within a ±10 % band. Figure 8 shows the analytical-calculated losses with respect to the rotational speed. The model suggests a total power loss of 19.4 W at a rotational speed of 168 krpm (blue squares), consisting of the journal bearing losses of 7.4 W (dashed-dotted red line), the windage losses of 4.4 W (dashed red line), and the thrust bearing loss of 7.6 W (dotted red line). Figure 5 gives an overview of the losses close to the fan side: The thrust bearing consists of a plain part from a radius 5 mm to 8 mm and a grooved part from 8 mm to 9.4 mm (dotted line) and the journal bearing loss consists of both journal bearings (Figure 5 shows one journal bearing with a dashed-dotted line). The windage losses (dashed lines) consist of losses of the following components: (1) fan windage loss, (2) shaft windage loss (partially marked in Figure 5), and (3) windage losses at the turbine side (not shown in Figure 5).

INFLUENCE OF LEAKAGE AND HEAT ON THE FAN POWER AND EFFICIENCY

Figure 9 shows the comparison between the measured isentropic total to total fan efficiencies and power as defined in eqs. (2) to (4). The experiments mean ambient pressure was 0.965 bar ± 0.004 bar, the total fan inlet temperature 200 °C ± 2 °C, and the rotational speed 50 krpm, 70 krpm, ..., 150 krpm, and 168 krpm ± 1 krpm. Correlations from ISO 5801 [9] adjust all experiments to a constant rotational speed, a constant ambient pressure (0.96 bar), and a constant fan inlet total temperature (200 °C).

The isentropic efficiency 1 and power 1 according to eq. (2) are directly evaluated based on the measured data. The fan power is calculated with the measured fan inlet mass flow rate ($\dot{m}_1$). Isentropic efficiency 2 and power 2 according to eq. (3) take the influence of the leakage mass flow rate into account. The leakage specific total enthalpy ($h_{t,l}$) is determined using the housing temperature (T_h) and the housing pressure (p_h). It is assumed that this enthalpy is constant until the leakage flow enters the fan fluid domain at the fan TE. As pointed out in the previous section, the maximum theoretically possible leakage mass flow rate ($\dot{m}_l$) with a discharge coefficient of 1 (blue line in Figure 7) is used. The fan outlet mass flow rate is calculated with this leakage mass flow rate ($\dot{m}_8 = \dot{m}_1 + \dot{m}_l$). The influence of the leakage rate on the measured fan power and efficiency ranges between +1 % and +0.2 % and is thus very small. As a consequence it is suggested that the effect of the leakage flow rate on the measurements can be neglected. The isentropic efficiency 3 and power 3 according to eq. (4) take into account heat input from the thrust bearing losses. Here it is assumed that 50 % of the dissipated heat due to the axial bearing losses is conducted to the stator part, whereas the other 50 % of the heat is conducted to the fan impeller and thus in the fan fluid domain. As shown in Figure 8 the heat dissipation ranges between 0.9 W/2 at 50 krpm and 7.6 W/2 at 168 krpm. With respect to the measured fan power (1.3 W at 50 krpm and 19.0 W at 168 krpm), the thrust bearing heat dissipation is suggested to have significant influence on power and efficiency measurements. Heat addition to the fan flow increases the measured fan power (P_1) and thus decreases the measured

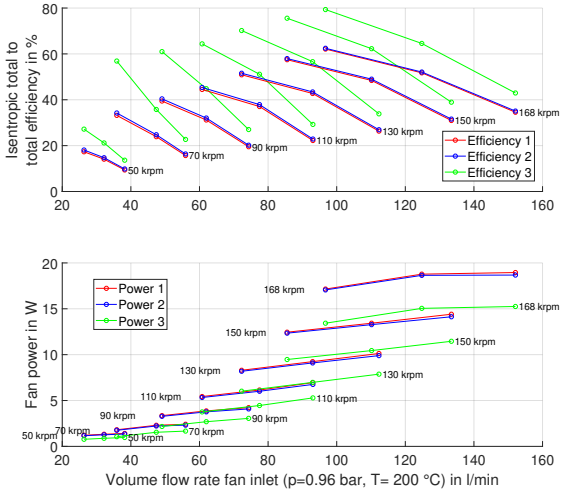

FIGURE 9. COMPARISON OF DIFFERENT EFFICIENCY AND POWER DEFINITIONS.

isentropic fan efficiency (η_1). While taking the heat addition effect into account, the net fan power is decreased (P_3) and thus the isentropic fan efficiency with heat addition correction is increased (η_3). The difference between η_1 and η_3 is between 4.3 % points at 50 krpm up to 23.7 % points at 70 krpm. It is noticed that a heat loss to the environment ($\dot{Q}_{amb}$) that is neglected within this study would have the opposite effect. It would decrease the measured power (P_1) and thus increase the measured efficiency (η_1).

NUMERICAL SIMULATION SETUP

A three-dimensional stationary CFD simulation with the commercial software *ANSYS CFX* simulates the fan performance that is compared to the experimental results. Figure 10 shows the entire fluid domain between the fan inlet and outlet temperature measurement locations: the inlet side test section (blue), the full fan impeller (red), the fan volute (orange), and the outlet side test section (green). The CFD simulation uses an unstructured mesh with 13.4 million tetrahedron elements for the fan and volute domain. The geometry assumes the running clearance 140 µm (150 µm-10 µm) at 168 krpm for all points. A fan impeller FEM simulation suggests that the axial blade elongation at the TE ranges between 3 µm to 10 µm, whereas it is close to 0 at the leading edge. As consequence, mechanical blade deformation is neglected. The 140 µm blade tip clearance is resolved with 3 elements within the gap. Correlations from ISO 5167 [10] evaluate the pressure loss at the bellmouth, and correlations from ISO 5801 [9] evaluate the pressure loss inside the fan inlet nozzle until the actual inlet of the CFD domain (red fan impeller domain). The fan impeller fluid domain is rotating with the corresponding rotational speed and features a frozen rotor fluid to fluid interface between the fan impeller outlet and the volute. The impeller shroud is a counter-rotating with respect to the rotating domain.

At the inlet, a temperature of 200 °C and a total pressure of 0.96 bar are specified corresponding to the experimental setup. At the outlet, the experimentally measured fan inlet mass flow rate is imposed (as stated before, the leakage effect is neglected). This measured fan inlet mass flow is adjusted to an inlet temperature of 200 °C, an inlet pressure of 0.96 bar, and the respective rotational speed (50 krpm, 70 krpm, ..., 150 krpm, and 168 krpm) as suggested in ISO 5801. All the wetted surfaces are considered as hydraulically smooth. Hence, surface roughness is not defined and skin friction loss is only caused by fluid viscosity. The area-averaged y-plus values inside the volute, impeller hub, impeller shroud, and impeller blades are maintained below 9, 7, 12, respectively 5. All walls are modeled as adiabatic. The CFD uses a compressible and non-isothermal ideal gas (air). The advection sheme is set to high resolution. The SST turbulence model with a low turbulence intensity of 1 % at the inlet boundary is specified. The total to total isentropic efficiency is evaluated between the inlet and outlet boundary as the mass-flow-averaged isentropic

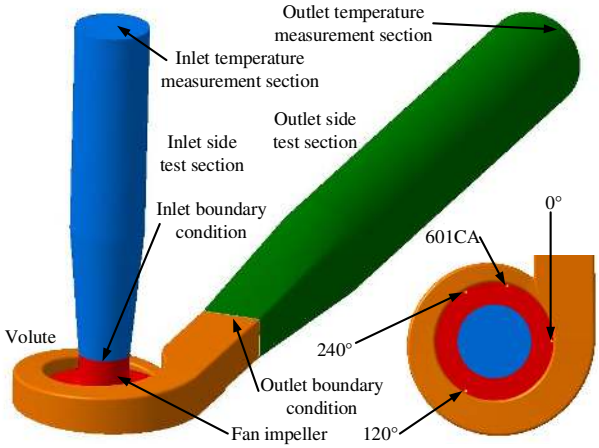

FIGURE 10. FLUID DOMAIN OF THE MEASUREMENT (BLUE, RED, ORANGE, AND GREEN), FOR THE COMPUTATIONAL FLUID DYNAMIC SIMULATION (RED AND ORANGE), AND POSITION OF STATIC PRESSURE TABS AT THE FAN TRAILING EDGE (0°, 120°, 240°, AND BLADE PASSING FREQUENCY 601C).

efficiency as defined in eq. (2) at the outlet boundary corresponding to the volute outlet. The total to total fan pressure increase is based on the mass-flow-averaged total pressure at the outlet boundary minus the ambient pressure of 0.96 bar and minus the calculated pressure loss of the inlet side test section. The pressure loss of the outlet side test section is therefore neglected. The fan TE shroud pressure corresponds to the area-averaged static pressure at the fan TE (diameter of 19.2 mm) minus the calculated pressure loss of the inlet side test section. The fan power is evaluated as the impeller torque (blades and hub) around the rotational axis multiplied with its angular velocity.

COMPARISON OF THE EXPERIMENTAL RESULTS TOWARDS THE DESIGN POINT AND NUMERICAL RESULTS

Figure 11 shows the fan characteristic with the total to total isentropic efficiency ($\eta_{is,1}$), the total to total fan pressure rise, the static gauge pressure at the fan impeller shroud at a diameter of 18.55 mm close to the fan TE for the 0°, 120°, and 240° locations (see Figure 10), the housing gauge pressure, as well as the fan power (P_1). As stated before, correlations from ISO 5801 [9] adjust all experimental values to a constant rotational speed, a constant ambient pressure (0.96 bar), and a constant total fan inlet temperature (200 °C).

The nominal speed line (168 krpm) has the same Mach number based on the total inlet conditions as the design case (SOFC anode off-gas consisting of water vapor, hydrogen, carbon monoxide, and carbon dioxide) and is therefore representative of the op-

eration when coupled to the SOFC. A black dot marks the nominal design point. At nominal operation, the total to total pressure increase is 55 mbar and therefore 15 mbar lower than the specified fan total total pressure increase. This difference has three reasons: (1) Since the current test campaign features a 100 µm shim, the clearance is elevated hence the isentropic efficiency and thus the fan pressure increase are lower compared to the nominal design clearance (50 µm). A numerical investigations with the design clearance of 50 µm suggests that the fan pressure rise increases by around 25 mbar to 80 mbar. (2) For a fan inlet total pressure of 1.05 bar instead of 0.96 bar, the pressure increase is according to ISO 5801 [9] 87.5 mbar ($\frac{1.05}{0.96}$80 mbar). (3) The anode off-gas has a lower heat capacity ratio (1.3) than air (1.4), wherefore the pressure rise is lower although the Mach number is constant. The pressure rise is therefore approximately equal to the initially specified 70 mbar with the design clearance (50 µm). At the design point, the volute was designed with respects to conservation of the circumferential velocity and constant volute pressure which is in agreement with the experimental data, since the difference between the measured fan TE shroud pressure at 0°, 120°, and 240° is near to zero (see magenta lines in Figure 11 at a constant speed line of 168 krpm). At higher mass flow rates, the fluid is accelerated within the volute, leading to a static pressure drop at 0° and a rise at 240° and vice versa for for lower mass flow rates.

With respects to the experiments and the CFD simulations, the fan TE shroud pressure, as well as the total to total fan pressure rise yield a good match for the nominal point (center point at 168 krpm), as well as for the non-throttled point (right point at 168 krpm). Near the nominal operation, the measured efficiency and power of the CFD simulation and the experiment suggest an excellent agreement. The difference between the measured and simulated power is -0.3 W (1.6 %), respectively 0.9 % points for the isentropic efficiency. For the non-throttled case, the difference in power is -1.8 W what is equal to -10 % with respect to the measured value. The measured efficiency 1 (34.6 %) is therefore 10 % points lower than the simulated value. The simulated value (44.6 %) is therefore close to the efficiency 3 according to eq. (4) that is 43 %. A heat input into the fan fluid domain is thus not negligible at this point. At the throttled point (left point on the nominal 168 krpm speed line) the stationary CFD simulation does not fully capture the increasingly instationary fan flow. The difference in the total to total pressure difference is 5 mbar, whereas it is 4 mbar with respect to the simulated fan TE shroud pressure and the averaged measured value. At this point, the measured fan power with respect to the simulated value is underestimated, whereas the efficiency is overestimated. As the flow within the fan impeller, the volute, and the diffuser at the volute outlet is more turbulent, the heat transfer coefficient between the fluid and the outlet side test section tube is increased. Although the test rig uses a PTFE tube, the heat loss to the environment can not be neglected at this point. The measured outlet temperature

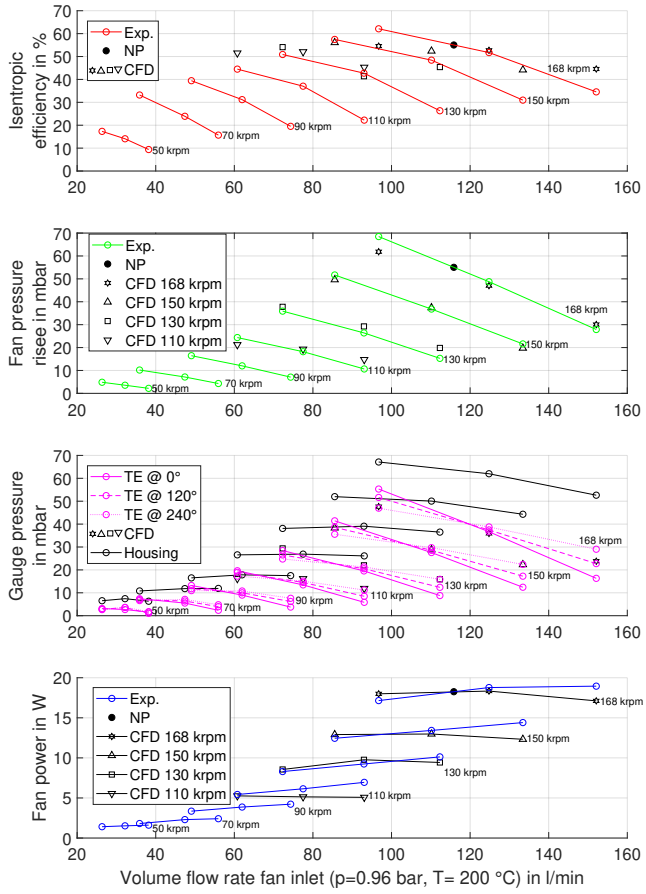

FIGURE 11. MEASURED FAN CHARACTERISTIC FROM EXPERIMENTS (EXP.), NOMINAL POINT (NP), AND COMPARISON TO CFD SIMULATION (CFD).

is therefore slightly decreased due to heat conduction within the PTFE tube to the environment.

The turbine uses air at 220 °C to drive the shaft and thus the fan impeller. The higher the shaft power, the higher the turbine inlet pressure, the higher the expansion within the turbine, and the lower the turbine outlet temperature. Below rotational speeds of 120 krpm the turbine outlet temperature is higher than 200 °C and thus above the oven environment temperature and the fan inlet temperature of 200 °C. The heat conduction from the turbine to the fan and the dissipated heat due to bearing losses crossing the fan fluid domain are therefore higher compared to rotational speeds above 120 krpm. The measured power and efficiency for rotational speeds at 50 krpm, 70 krpm, 90 krpm, and 110 krpm are therefore influenced by increased heat fluxes crossing the fan fluid domain. The difference in the isentropic efficiency is between 7.0 % points for the throttled case up to 23.1 % points for the non-throttled case for the 110 krpm speed line. The center point and left point (throttled case) of the 130 krpm and 150 krpm

case show better agreement ($\pm 4\,\%$ points), since the heat fluxes crossing the fan impeller domain are lower.

CONCLUSION

A novel AOR fan for a $10\,\mathrm{kW_e}$ Solid Oxide Fuel Cell (SOFC) was designed, manufactured, experimentally characterized, and its performance compared to a Computational Fluid Dynamic (CFD) simulation. This fan uses dynamic gas-lubricated bearings, more specifically herringbone-grooved journal and spiral-grooved thrust bearings that have proven to be reliable, even at elevated temperature of up to $220\,^{\circ}\mathrm{C}$. The design of the fan is based on a trade-off between efficiency and low manufacturing cost. Due to the high rotational speeds, the fan performance corresponds to the specified values, although the size is out of the common. The fan blade tip clearance is suggested to have a significant impact also for fans with relatively low pressure rises.

At the nominal point at 168 krpm, the measured inlet mass flow rate is $4.9\,\mathrm{kg\,h^{-1}}$, the total to total pressure rise reaches 55 mbar, yielding an isentropic total to total efficiency 55 %, and a power of 18.3 W.

The influence of leakage mass flow rate from the housing to the fan trailing edge causes a theoretical maximum deviation in the measured isentropic total to total efficiency of 0.2 % to 1 % points and can therefore be neglected within the experiments and simulations. A possible heat input to the fan flow due to the axial thrust bearing losses has the potential of influencing the total to total isentropic efficiency measurement by up to 24 % points and is therefore not negligible. An adiabatic CFD simulation is compared to the measurements.

At the nominal point, the difference between the experimentally measured and simulated values for the isentropic total to total efficiency is +0.9 % points, for the fan power -0.3 W, for the fan total to total pressure difference -0.7 mbar, and for the averaged static pressure at the fan trailing edge -1.7 mbar. It is thus concluded that the proposed experimental set up is suitable for characterizing the fan at the nominal operational point although its power is in the same order as the shaft losses. At this point, the majority of the dissipated heat cross a heat sink that is the cold turbine fluid domain in this case. An isolation with glass fiber tapes and a PTFE tube reduce the heat conduction to the (oven) environment. However, at off-design conditions, the dissipated heat, respectively the heat loss to the environment have more significant impact. The precise determination of the entire fan characteristic remains therefore challenging.

ACKNOWLEDGMENT

The authors acknowledge the research grant from the Canton de Vaud under the “100 million de francs pour les energies renouvelables et l’efficacite energetique”.

REFERENCES

[1] SOLIDpower, 2016. BlueGen datasheet. http://www.solidpower.com/fileadmin/user_upload/pages/Logos_materialien/SOLIDpower_BlueGEN_Brochure_UK_web.pdf. Accessed: 2018-06-16.

[2] Jülich Forschungszentrum, 2017. Anniversary for Jülich’s Slow Burner: Fuel Cell Running for 10 Years. https://www.fz-juelich.de/SharedDocs/Pressemitteilungen/UK/EN/2017/2017-08-07-jubilaeum-sofc.html. Accessed: 2018-06-22.

[3] Wagner, P. H., Wuillemin, Z., Diethelm, S., Van herle, J., and Schiffmann, J., 2017. “Modeling and Designing of a Radial Anode Off-Gas Recirculation Fan for Solid Oxide Fuel Cell Systems”. *Journal of Electrochemical Energy Conversion and Storage,* ***14***(1), May, pp. 011005–011005–12.

[4] Peters, R., Engelbracht, M., Tiedemann, W., Hoven, I., Deja, R., Nguyen, V. N., Blum, L., and Stolten, D., 2017. “Development and Test of a Solid Oxide Fuel Cell Subsystem with a Low Temperature Anode Off-Gas Recirculation”. *ECS Transactions,* ***78***(1), May, pp. 2489–2495.

[5] GE Power, 2018. Breaking the Power Plant Efficiency Record...Again! https://www.ge.com/power/about/insights/articles/2018/03/nishi-nagoya-efficiency-record, Mar.

[6] Wagner, P. H., Wuillemin, Z., Diethelm, S., Van herle, J., and Schiffmann, J., 2019. “Design of a Small-Scale, High-speed, and Oil-free Radial Anode Off-Gas Recirculation Fan for Solid Oxide Fuel Cell Systems”. In Proceedings of 13th European Conference on Turbomachinery Fluid dynamics.

[7] Agrawal, G., 2010. Advances in fuel cell blowers. www.netl.doe.gov/file%20library/events/2009/seca/presentations/Agrawal_Presentation.pdf. Accessed: 2015-04-14.

[8] Heshmat, H., 2016. High Temperature Anode Recycle Blower for Solid Oxide Fuel Cell. Tech. rep., Mohawk Innovative Technology, https://www.netl.doe.gov/research/coal/project-information/proj?k=FE0027895.

[9] ISO, 2007. ISO 5801: Industrial fans - Performance testing using standardized airways.

[10] ISO, 2003. ISO 5167: Measurement of fluid flow by means of pressure differential devices inserted in circular cross-section conduits running full.

[11] VDI, 1991. VDI/VDE 2041: Measurement of Fluid Flow with Priminary Devices - Orifice Plates and Nozzles for Special Applications.

[12] Demierre, J., Rubino, A., and Schiffmann, J., 2014. “Modeling and Experimental Investigation of an Oil-Free Microcompressor-Turbine Unit for an Organic Rankine Cycle Driven Heat Pump”. *Journal of Engineering for Gas Turbines and Power,* ***137***(3), Oct.

